stable coronary artery disease and ventricular dysfunction. *J Nucl Med* 1997;38:419–424.
6. Udelson JE, Coleman PS, Metherall J, et al. Predicting recovery of severe regional ventricular dysfunction: comparison between resting scintigraphy with ^{201}Tl and ^{99m}Tc-sestamibi. *Circulation* 1994;89:2552–2561.
7. Sansoy V, Glover DK, Watson DD, et al. Comparison of thallium-201 resting redistribution with technetium-99m-sestamibi uptake and functional response to dobutamine for assessment of myocardial viability. *Circulation* 1995;92:994–1004.
8. Dilsizian V, Arrighi JA, Diodati JG, et al. Myocardial viability in patients with chronic ischemic left ventricular dysfunction: comparison of ^{99m}Tc-sestamibi, ^{201}thallium, and ^{18}F-fluorodeoxyglucose. *Circulation* 1994;89:578–587.
9. Altehoefer C, vom Dahl J, Biedermann M, et al. Significance of defect severity in technetium-99m-MIBI SPECT at rest to assess myocardial viability: comparison with fluorine-18-FDG PET. *Eur J Nucl Med* 1994;35:569–574.
10. Dilsizian V, Perrone-Filardi P, Arrighi JA, et al. Concordance and discordance between stress-redistribution-reinjection and rest-redistribution thallium imaging for assessing viable myocardium. Comparison with metabolic activity by positron emission tomography. *Circulation* 1993;88:941–952.
11. Sawada S, Allman K, Muzik O, et al. Positron emission tomography detects evidence of viability in rest technetium-99m-sestamibi defects. *J Am Coll Cardiol* 1994;23:92–98.
12. Schelbert HR. Blood flow and metabolism by PET. In: Verani MS, Crawford MH, eds. *Cardiology Clinics. Nuclear Cardiology.* Philadelphia, PA: WB Saunders; 1994:12: 303–315.
13. Tillisch JH, Brunken R, Marshall R, et al. Reversibility of cardiac wall motion abnormalities predicted by positron tomography. *N Engl J Med* 1986;314:884–888.
14. Knapp FF Jr, Ambrose KR, Goodman MM. New radioiodinated methyl branched fatty acids for cardiac studies. *Eur J Nucl Med* 1986;12(suppl):S39–S44.
15. Franken PR, De Geeter F, Dendale P, Demoor D, Block P, Bossuyt A. Abnormal free fatty acid uptake in subacute myocardial infarction after coronary thrombolysis: correlation with wall motion and inotropic reserve. *J Nucl Med* 1994;35:1758–1765.
16. De Geeter F, Franken PR, Knapp FF, Bossuyt A. Relationship between blood flow and fatty acid metabolism in subacute myocardial infarction: a study by means of ^{99m}Tc-sestamibi and ^{123}I-β-methyl-iodo-phenyl pentadecanoic acid. *Eur J Nucl Med* 1994;21:283–291.
17. Ito T, Tanouchi J, Kato J, et al. Recovery of impaired left ventricular function in patients with acute myocardial infarction is predicted by the discordance in defect size on ^{123}I-BMIPP and ^{201}Tl-SPECT images. *Eur J Nucl Med* 1996;23:917–923.
18. Franken PR, Dendale P, De Geeter F, Demoor D, Bossuyt A, Block P. Prediction of functional outcome after myocardial infarction using BMIPP and sestamibi scintigraphy. *J Nucl Med* 1996;37:718–722.
19. Tamaki N, Kawamoto M, Yonekura Y, et al. Regional metabolic abnormality in relation to perfusion and wall motion in patients with myocardial infarction: assessment with emission tomography using an iodinated branched fatty acid analog. *J Nucl Med* 1992;33:659–667.
20. Tamaki N, Tadamura E, Kudoh T, et al. Prognostic value of iodine-123-labelled BMIPP fatty acid analogue in patients with myocardial infarction. *Eur J Nucl Med* 1996;23:272–279.
21. Mertens J, Eersels J, Van Ryckeghem W. New high yield Cu(I) assisted I-123 radioiodination of 15(p-I-phenyl)-9-methyl pentadecanoic acid, a potential myocardial tracer. *Eur J Nucl Med* 1987;13:159–160.
22. Van Steelandt E, Dobbeleir A, Vanregemorter J. Compton scatter correction for scintigraphic imaging. *Proceedings of the 11th annual symposium of the Belgian Association of Hospital Physicists.* Ghent, Belgium: University of Ghent; 1995:23.
23. Goresky CA, Stremmel W, Rose CP, et al. The capillary transport system for free fatty acids in the heart. *Circ Res* 1994;74:1015–1026.
24. Fujibayashi Y, Yonekura Y, Takemura Y, et al. Myocardial accumulation of iodinated beta-methyl branched fatty acid analogue, iodine-125-15-(p-iodophenyl)-3-(R,S) methyl pentadecanoic acid (BMIPP) in relation to ATP concentration. *J Nucl Med* 1990;31:1818–1822.
25. Yamamichi Y, Kusuoka H, Morishita K, et al. Metabolism of iodine-123-BMIPP in perfused rat hearts. *J Nucl Med* 1995;36:1043–1050.
26. Fujiwara S, Takeishi Y, Atsumi H, Takahashi K, Tomoike H. Fatty acid metabolism imaging with iodine-123-BMIPP for the diagnosis of coronary artery disease. *J Nucl Med* 1997;38:175–180.
27. Bax JJ, Wijns W, Cornel JH, Visser FC, Boersma E, Fioretti PM. Accuracy of currently available techniques for prediction of functional recovery after revascularization in patients with left ventricular dysfunction due to coronary artery disease: comparison of pooled data. *J Am Coll Cardiol* 1997;30:1451–1460.
28. Tateno M, Tamaki N, Yukihiro M, et al. Assessment of fatty acid uptake in ischemic heart disease without myocardial infarction. *J Nucl Med* 1996;37:1981–1985.
29. Arnese M, Cornel JH, Salustri A, et al. Prediction of improvement of regional left ventricular function after surgical revascularization. *Circulation* 1995;91:2748–2752.
30. McGillem MJ, DeBoe SF, Friedman HZ, Mancini GBJ. The effects of dopamine and dobutamine on regional function in the presence of rigid coronary stenoses and subcritical impairments of reactive hyperemia. *Am Heart J* 1988;115:970–977.
31. Sklenar J, Ismail S, Villanueva FS, Goodman NG, Glasheen WP, Kaul S. Dobutamine echocardiography for determining the extent of myocardial salvage after reperfusion. *Circulation* 1994;90:1502–1512.
32. Panza JA, Dilsizian V, Laurienzo JM, Curiel RV, Katsiyiannis PT. Relation between thallium uptake and contractile response to dobutamine: implications regarding myocardial viability in patients with chronic coronary artery disease and left ventricular dysfunction. *Circulation* 1995;91:990–998.
33. Beller GA. Comparison of ^{201}Tl scintigraphy and low dose dobutamine echocardiography for the noninvasive assessment of myocardial viability. *Circulation* 1996;94: 2681–2684.

Effect of Oral Glucose Loading on the Biodistribution of BMIPP in Normal Volunteers

Frank De Geeter, Vicky Caveliers, Ingrid Pansar, Axel Bossuyt and Philippe R. Franken
Department of Nuclear Medicine, University Hospital, Free University Brussels, Brussels, Belgium

We have evaluated whether myocardial uptake of the fatty acid analog ^{123}I-15-(p-iodophenyl)-3-R,S-methyl pentadecanoic acid (BMIPP) is dependent on the dietary state. **Methods:** We compared the biodistribution of 150 MBq of ^{123}I-BMIPP in six healthy volunteers in two states: after at least 12 hr of fasting and after oral glucose loading (75 g) 60 min before tracer administration, followed by a meal enriched in carbohydrates and protein. Planar and tomographic acquisitions were performed over a 4-hr time period after tracer injection; data were corrected for radioactive decay and injected dose. Radioactivity was measured in blood samples drawn at several points. **Results:** Significant increases of glycemia and insulinemia and a significant drop in plasma nonesterified acids were documented after glucose loading. Half-time values for plasma radioactivity were significantly shorter in the glucose-loaded state than in the fasted state (4.3 ± 1.4 min compared to 6.3 ± 1.3 min, $p < 0.05$). Activity in the heart and liver tended to be higher in the glucose-loaded state than in the fasted state. SPECT images at 0.5 hr after tracer injection demonstrated that the myocardial wall-to-cavity ratio was higher after glucose than in the fasted state (2.53 ± 0.59 compared to 2.11 ± 0.21, $p = 0.15$). Washout from the liver between 1 and 4 hr after injection increased from 18.6% ± 4.4% in the fasted study to 24.1% ± 2.4% after glucose ($p = 0.04$). Washout from the myocardium between 0.5 and 3.5 hr after injection increased from 13.1% ± 8.8% in the fasted study to 24.0% ± 3.7% after glucose ($p = 0.05$). **Conclusion:** These results indicate that fasting before BMIPP scintigraphy is not mandatory to obtain adequate SPECT images. At the time when SPECT is usually performed, glucose loading may provide improved ratios between myocardial and blood pool activity.

Key Words: 15-(p-iodophenyl)-3-R,S-methyl pentadecanoic acid; glucose; biodistribution

J Nucl Med 1998; 39:1850–1856

The clinical utility of ^{123}I-labeled 15-(p-iodophenyl)-3-R,S-methyl pentadecanoic acid (BMIPP) in cardiomyopathy as well as in ischemic heart disease has been documented extensively (*1,2*). In ischemic heart disease, evidence has accumulated that myocardial areas in which the uptake of BMIPP is diminished

Received Oct. 1, 1997; revision accepted Feb. 12, 1998.
For correspondence or reprints contact: Frank De Geeter, MD, Department of Nuclear Medicine, AZ-VUB, Laarbeeklaan 101, B-1090 Brussels, Belgium.

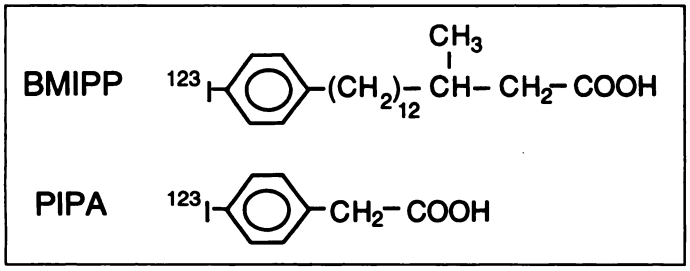

FIGURE 1. Chemical structures of BMIPP and the end product of its metabolism, PIPA.

relative to perfusion tracers (termed mismatches) are indicative of jeopardized myocardium, which is often dysfunctional (*3,4*) but is fully capable of recovery (*5,6*). This stands in contradiction to areas with equally suppressed BMIPP and flow tracer activity, which generally are scarred.

After an energy-requiring activation, the largest part of BMIPP is subsequently stored in the cytosolic triglyceride pool, because the methyl group in beta position inhibits entry of the activated fatty acid into beta-oxidation (*7*). However, a small part of BMIPP is metabolized through successive alpha- and beta-oxidation, finally leading to the production of p-iodophenyl-acetic acid (PIPA) (Fig. 1) (*8,9*). BMIPP effectively traces the uptake into the cell and the activation of fatty acids (*10,11*); indirectly, it reflects cellular adenosine triphosphate content (*12*).

In analogy to studies with straight-chain analogs, it has become standard practice to perform BMIPP studies after an overnight fast. In contrast to BMIPP, however, straight-chain analogs assess beta-oxidation and, accordingly, should be administered in conditions that favor fatty acid oxidation. The effect of metabolic milieu on the biodistribution of BMIPP in normal volunteers has not been previously addressed. The aim of this study, therefore, was to investigate how metabolic conditions affect the biodistribution of BMIPP and the resulting image quality.

MATERIALS AND METHODS

Study Population

We investigated six healthy male volunteers. Their ages ranged from 19 to 25 yr. Informed consent was obtained, and the study protocol was approved by the institutional ethical review board.

Synthesis of BMIPP

BMIPP was purchased from Emka-Chemie (Markgröningen-Talhausen, Germany) and radioiodinated with ^{123}I(p, 5n) using a high-yield Cu(I)-assisted radioiodination method described previously (*13*). This labeling procedure yields 75% ^{123}I-BMIPP, with a radiochemical purity of >97%. The final product had a specific activity of >200 GBq/mmol and was formulated in 6–8 ml of a 4% human serum albumin solution in saline.

Study Protocol

All of the volunteers were imaged twice. The first set of acquisitions was performed after an overnight fast of at least 12 hr. The second time, 1 wk later, the same set of acquisitions was repeated after an oral glucose load of 75 g, followed by a meal enriched in carbohydrates and protein content. This meal contained 70 g of carbohydrates, 41 g of protein and 21 g of fat, for a total of 610 calories, and was consumed 30 min after the glucose load. It was given for the purpose of sustaining the metabolic changes induced by the glucose load for as long as possible (*14*). Approximately 1 hr before tracer administration, intravenous catheters were placed in each arm, one to be used for tracer injection and the other for blood sampling. For the glucose-loaded study, BMIPP was injected ~1 hr after oral glucose administration.

Plasma Analysis

Glucose, Insulin and Nonesterified Fatty Acid Concentrations. At the time of glucose administration, tracer injection and again 30, 60 and 90 min later, blood was drawn in serum tubes, to measure the levels of glucose, insulin and nonesterified fatty acids (NEFAs). Glucose was determined with the glucose oxidase method (Johnson and Johnson Clinical Diagnostics, Rochester, NY). Insulin was assessed with a radioimmunometric assay (Medgenix Diagnostics, Fleurus, Belgium). NEFAs were measured by enzymatic colorimetric methods (NEFA C ACS-ACOD; Wako Chemicals, Neuss, Germany).

Total Radioactivity and Chromatographic Analysis. Blood samples were drawn into heparinized syringes at ~2, 5, 10, 15, 20, 30, 60 and 90 min and at 4 hr after tracer administration. Plasma activity was measured on 1-ml samples in a well counter (Cobra II Inspector 5003, Canberra-Packard, Meriden, CT). By comparison to a standard, activity was expressed as a percentage of the injected dose (%ID).

The rest of the plasma was acidified with hydrochloride and extracted with a 2:1 mixture of chloroform and methanol. The organic phase was evaporated to dryness, and the residue was dissolved in 500 μl of eluents for high-performance liquid chromatography analysis. BMIPP, PIPA and other metabolites were separated on a Lichrospher RP8 column using a mixture of methanol:water:acetic acid (85:15:0.5) at a flow rate of 1 ml/min. The detected radioactive peaks were quantified by integrating the output of the single channel analyzer. Metabolites were identified by comparison of their retention times with those of authentic standards injected simultaneously.

Planar Imaging

Approximately 150 MBq of ^{123}I-BMIPP was injected intravenously at rest, with the patient lying supine. All scintigraphies were acquired on a dual head gamma camera system (MultiSPECT2; Siemens, Chicago, IL), fitted with medium-energy collimators (*15*). A 20% pulse height window was centered on the 159-keV photopeak of ^{123}I. Figure 2 depicts the sequence of the various acquisitions.

Acquisition. Before injection of the tracer, the detectors were positioned over the thoracic and the higher abdominal (liver) regions. Injection was followed immediately by a dynamic study, consisting of 10-sec frames over 5 min followed by 20-sec frames over the next 10 min. The matrix size was 64 × 64. No zoom was applied.

Static images of 60-sec duration were acquired into a 64 × 64 matrix at ~60, 105, 200 and 270 min after tracer administration, using the same camera position as for the dynamic study. Whole-body studies were performed at ~1 and 4 hr after tracer injection. The detectors moved at a speed of 10 cm/min.

Processing. Irregular regions of interest were drawn manually over the heart and liver on geometric mean images; lung activity was sampled in a rectangular region of interest at the right lung basis, avoiding the nearby mediastinum and liver. The same regions were used throughout all the static studies for both the fasted and the glucose-loaded study, but their position was adjusted on each image to accommodate for displacement of the subjects between the various acquisitions.

On the whole-body studies, counts in the region over an organ were expressed as a percentage of the counts in the whole image. This quantity was used as an estimate of the %ID present in the organ at that point in time. The counting rates in the dynamic and static images were corrected for decay and normalized for acquisition time, to construct time-activity curves (TACs). These were then calibrated in %ID.

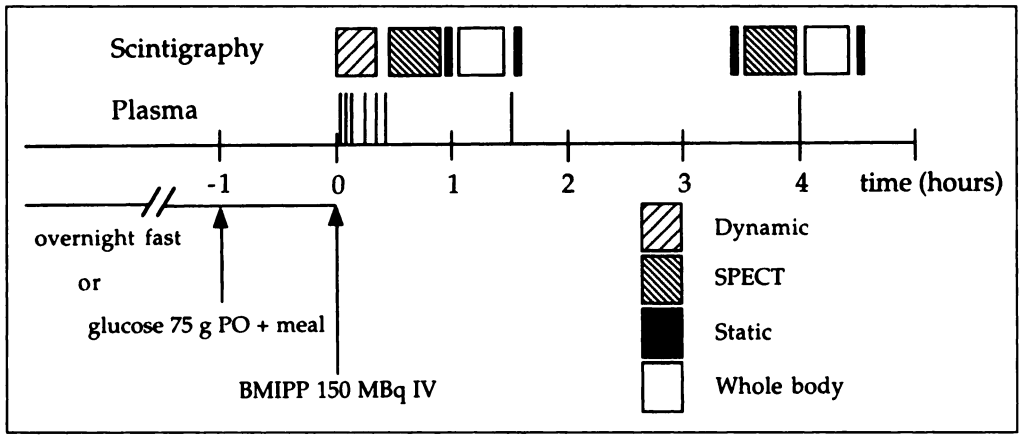

FIGURE 2. Time sequence for the acquisitions in the fasted and glucose-loaded states.

SPECT Imaging

Acquisition. SPECT of the heart was performed at ~0.5 hr and again at ~3.5 hr after tracer administration. Projection images were acquired into 64 × 64 matrices using a zoom factor of 1.78 in 32 positions of each detector (for a total of 64 projections over 360°) with a dwell time of 60 sec.

Processing. The SPECT studies were reconstructed using a Butterworth filter (order 7, cutoff frequency 0.4 Nyquist), without attenuation correction. Elliptical regions corresponding to the outer and inner contours of the myocardium were drawn on short-axis slices and were used on both the fasted and the glucose-loaded study. Myocardial activity was measured as the total counts between these ellipses, summed over the different slices representing the midventricular and basal regions. Blood activity in the cavity was sampled by the minimal pixel present in this region. Regional activity in the fasted and glucose-loaded state was compared on bull's-eye plots (*16*). Scores for septal, anterior, lateral and inferior regions were calculated as the mean of the subregions in that area. For the SPECT studies, washout was calculated between 0.5 and 3.5 hr.

Statistical Analysis

Results are expressed as the mean ± s.d. Comparisons between the fasted and glucose-loaded state were made using Wilcoxon's signed rank test or paired Student's t-tests, as appropriate. A p value of <0.05 was considered statistically significant.

RESULTS

Effects of Oral Glucose Load

Figure 3 illustrates the effects of the oral glucose load on plasma glucose, insulin and NEFAs. Glucose and insulin values increased from baseline values (95 ± 10 mg/dl and 12 ± 13 milliunits/liter, respectively) to a peak at the time of tracer injection (134 ± 40 mg/dl and 111 ± 52 milliunits/liter, respectively). Nonesterified fatty acids showed a marked drop (from 0.76 ± 0.41 to 0.08 ± 0.05 mEq/liter), which was sustained from the time of tracer administration over the next 90 min.

Plasma Activity Curves

Figure 4 presents the plasma total activity curves over 20 min (Fig. 4A) and 4 hr after tracer injection (Fig. 4B). The curves for the glucose-loaded state were always below those for the fasted state, although over time, both curves tended to come together. The differences reached statistical significance at 15 and 20 min after tracer injection. Plasma half-times were calculated by simple exponential fitting on the downsloping part of the curves, within 20 min after tracer administration. Half-time was significantly shorter in the glucose-loaded state (4.3 ± 1.4 min) than in the fasted state (6.3 ± 1.3 min, $p < 0.05$). Figure 4C and D depicts the plasma curves of BMIPP and PIPA. The activity of BMIPP decreased quickly and a slow buildup of PIPA in the plasma took place in both the fasted and the glucose-loaded state. For BMIPP as well as for PIPA, the mean values at all points in time were lower in the glucose-loaded state than in the fasted state, although the difference was not statistically significant.

Time-Activity Curves over the Liver and the Heart

Figure 5 illustrates the mean TACs in regions over the liver (Fig. 5A and B) and heart (Fig. 5C and D). At ~1 hr after tracer administration, activities in the heart were 4.67% ± 0.58%ID in the fasted state and 4.95% ± 0.67%ID in the glucose-loaded state (p = not significant); activities in the liver were 8.80% ± 1.91%ID in the fasted state and 9.57% ± 1.50%ID in the glucose-loaded state (p = not significant). Activity in both liver and heart was higher in the glucose-loaded state than it was in the fasted state, but the differences between both states were markedly less for the heart than for the liver. On the SPECT images, activity in the myocardium was 1.09 ± 0.11 times higher in the glucose-loaded state than in the fasted state (range 0.95–1.24).

Heart-to-Liver and Heart-to-Lung Ratios

Heart-to-liver ratios were significantly lower in the glucose-loaded state than in the fasted state at most time points between 2 and 12 min after tracer administration. Heart-to-lung ratios showed no statistically significant differences between the two

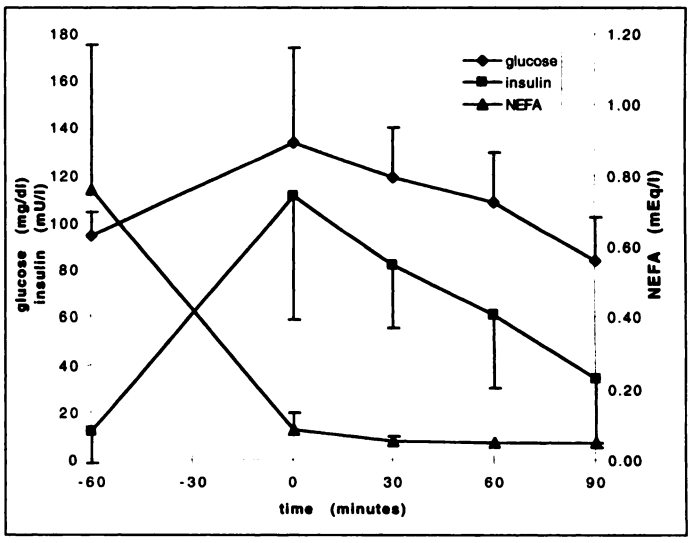

FIGURE 3. Effects of oral glucose load and meal on serum glucose, insulin and NEFAs. Time 0 corresponds to tracer injection; the glucose load and meal were given 60 min before.

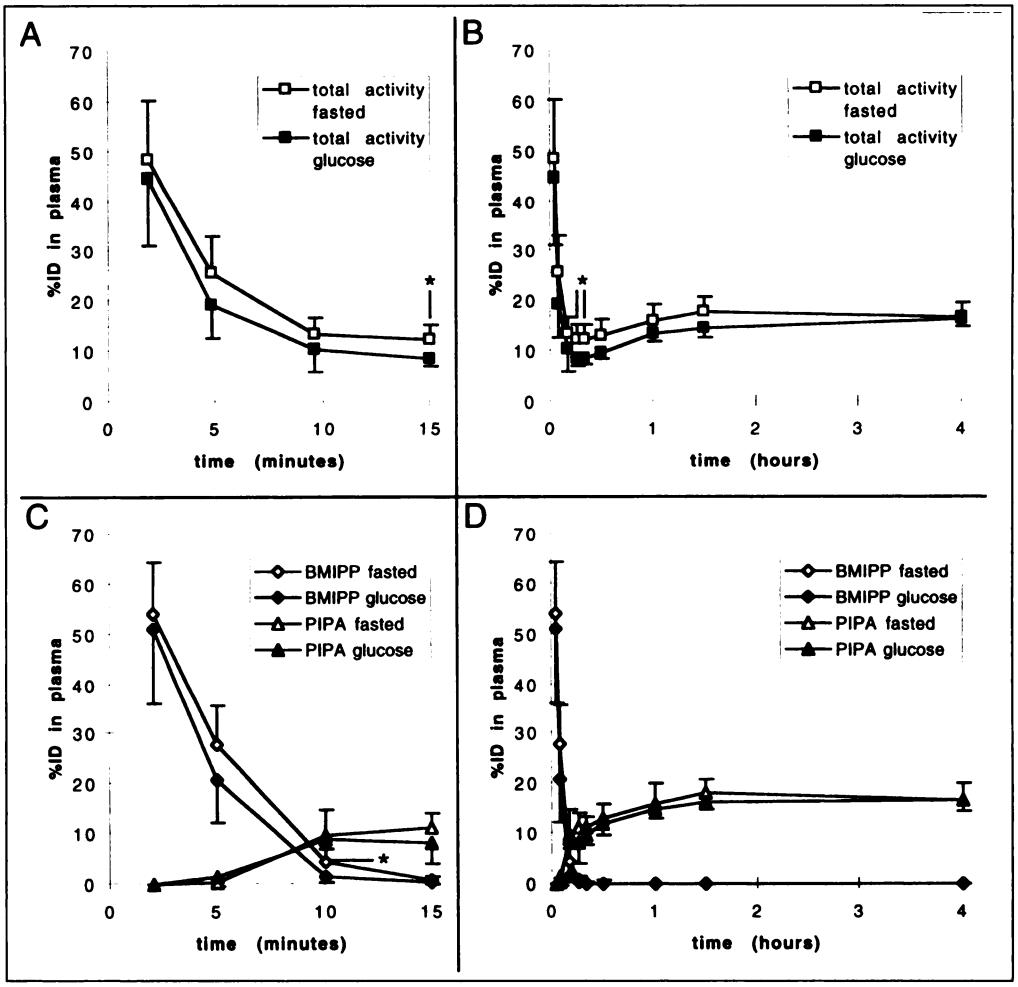

FIGURE 4. Plasma activity curves. (A and B) The total activity in the plasma is represented, in units of %ID in the estimated total plasma volume. (C and D) Activities of BMIPP and PIPA as determined by high-performance liquid chromatography are given. A and C depict activity curves for the first 15 min after tracer administration, whereas B and D extend over 4 hr. The mean values obtained in the six volunteers are used for the fasted and glucose-loaded states. *Statistically significant differences.

states, except at 4.5 hr after tracer administration, when they were higher after fasting.

Myocardium-to-Cavity Ratio on SPECT

Figure 6 shows a typical example of SPECT studies in the fasted and glucose-loaded state in a single volunteer. Blood pool activity in the cavity was lower but myocardial activity was higher in the glucose-loaded state. On planar images, these effects tended to cancel out, which accounts for the small differences observed for the heart TACs between the fasted and glucose-loaded state. Figure 7 illustrates that ratios of activity in the myocardial wall to activity in the cavity tended to be higher ($p = 0.15$) in the glucose-loaded early SPECT (2.53 ± 0.59) than in the fasted early SPECT (2.11 ± 0.21). On the late SPECT, these differences had disappeared (1.68 ± 0.31 in the fasted stated compared with 1.70 ± 0.25 in the glucose-loaded state, p = not significant).

Regional Myocardial Distribution on SPECT

The mean distribution of the tracer in the myocardium was not significantly different between the fasted and the glucose-loaded state. The mean scores for the septal, anterior, lateral and inferior wall were 85.9 ± 6.6, 91.4 ± 4.0, 91.1 ± 3.6 and 86.6 ± 7.4 in the fasted state and 87.0 ± 5.6, 89.7 ± 5.6, 92.2 ± 3.2 and 84.6 ± 5.1 in the glucose-loaded state, respectively.

Initial Washout

Figure 8 illustrates that washout from the organs during the first hours after injection is increased in the glucose-loaded state. For the liver, washout was higher in the glucose-loaded than in the fasted study (24.1% ± 2.4% compared to 18.6% ± 4.4%, $p = 0.04$). For the heart, washout was higher in the glucose-loaded study than in the fasted study (14.0% ± 2.8% compared to 10.7% ± 1.8%, $p = 0.06$). For the myocardium, as isolated on the SPECT images, this difference was even more marked: 24.0% ± 3.7% in the glucose-loaded study compared to 13.1% ± 8.8% in the fasted study ($p = 0.05$).

DISCUSSION

This study demonstrates that dietary state affects the biodistribution of BMIPP only to a minor degree.

Effect on Plasma Clearance

BMIPP cleared faster from the plasma in the glucose-loaded state than it did in the fasted state. Faster clearance from the plasma after glucose and insulin infusion has been observed with 1-^{11}C-beta-methylheptadecanoic acid, another methyl-branched fatty acid analog, in mongrel dogs (*17*). Because plasma clearance is the net result of uptake by the tissues and reflux of substrate or metabolites from the tissues, multiple factors may contribute to enhanced plasma clearance in the glucose-loaded state.

A major factor may relate to the suppressed circulating levels of fatty acids in the glucose-loaded state. Uptake of fatty acids into myocardium is known to display saturation kinetics, with K_m values in the range of 0.24 μmol/g (*18*). Therefore, decreased competition by fatty acids in the glucose-loaded state might cause higher uptake of the radiolabeled fatty acid into the tissues. To our knowledge, no measurements of the influence of feeding state on forward unidirectional tracer extraction have been published for BMIPP. However, higher one-way extraction of 14-iodophenyl-beta-methyltetradecanoic acid, a fatty

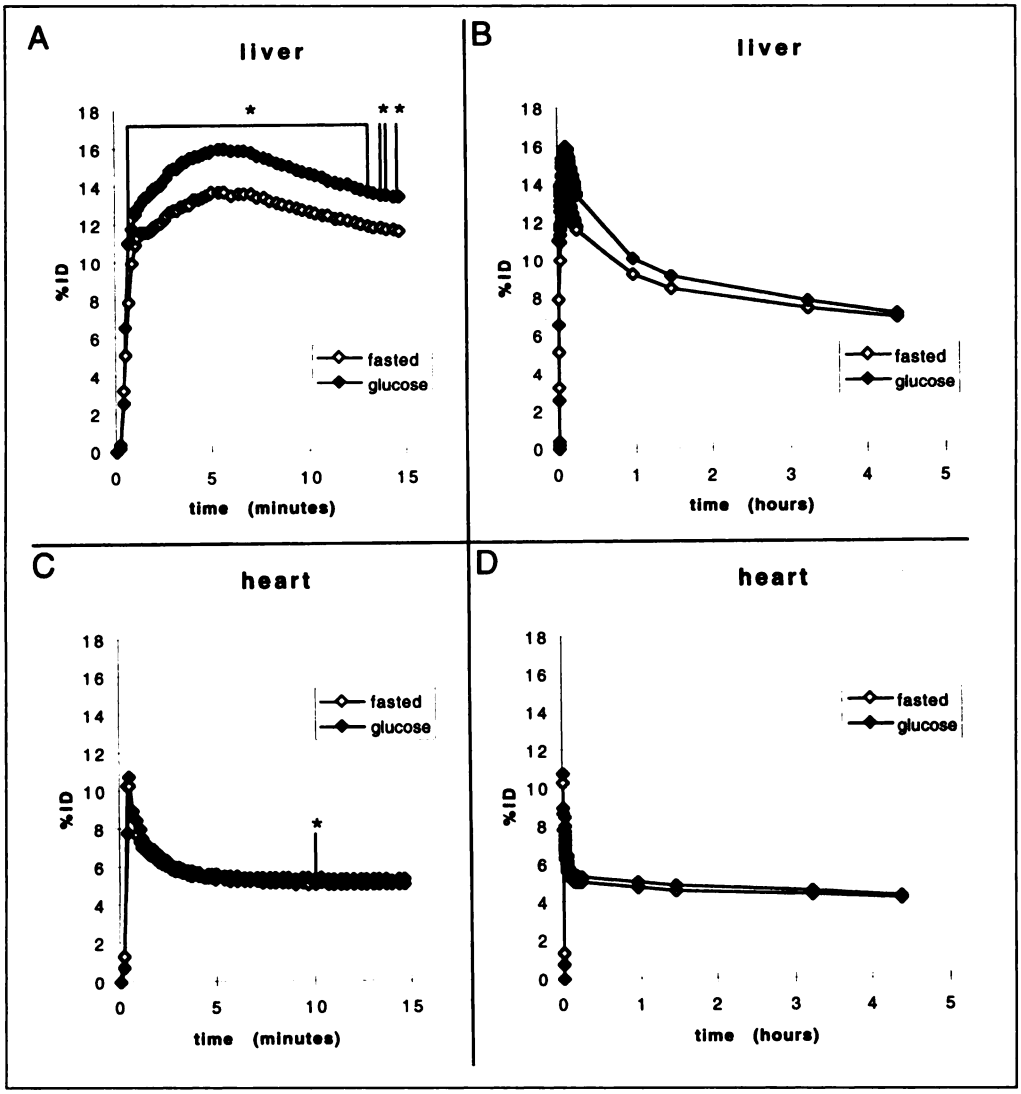

FIGURE 5. Organ TACs. A and B give the mean TACs over the liver, whereas C and D give the mean TACs over the heart. The time frames are the same as those in Figure 3. The ordinate uses the same scale for heart as for liver. *Statistically significant differences.

acid analog similar to BMIPP, was found in anesthetized greyhound dogs after intravenous infusion of glucose and insulin (0.44 ± 0.06 s.e.m.) than at baseline (0.38 ± 0.06 s.e.m.) (*19*). Conversely, forward extraction of ^{11}C-palmitate in mongrel dogs was lower after glucose/insulin infusion (0.38) than in control experiments (0.52) (*20*). The difference in this respect between palmitate and the methyl-branched tracers BMIPP and 14-iodophenyl-beta-methyltetra-

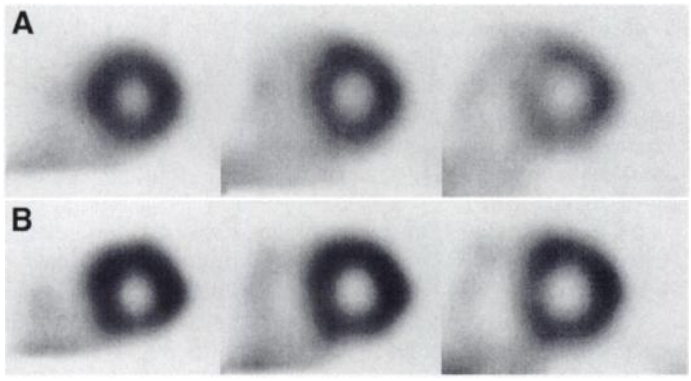

FIGURE 6. Typical example of early SPECT studies in fasted (A) and glucose-loaded (B) states from a single volunteer. These studies were obtained after injection of the same dose and are normalized to their common maximum. Note the increased myocardium/cavity contrast in the glucose-loaded state.

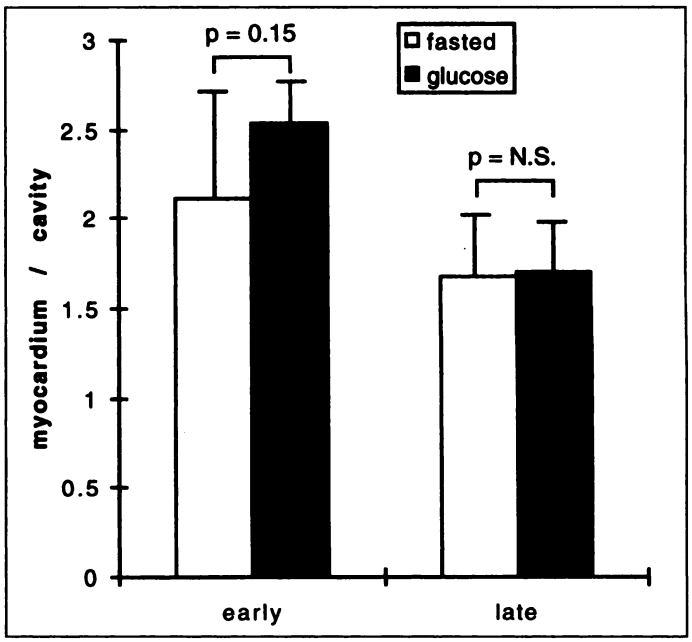

FIGURE 7. Myocardial wall-to-cavity ratio for the early and late SPECT studies. N.S. = not significant.

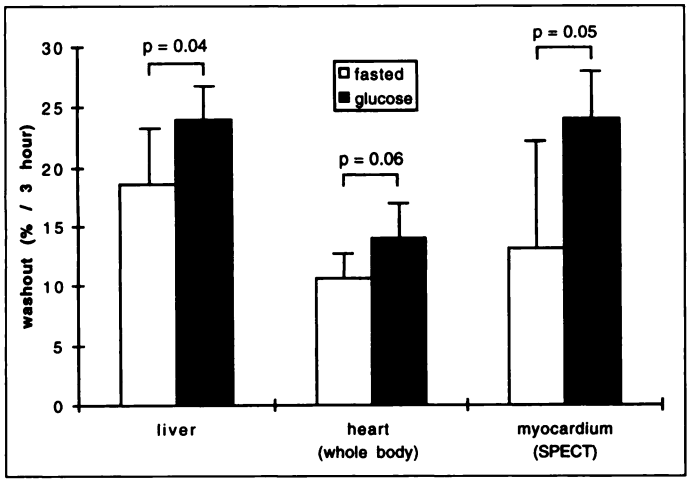

FIGURE 8. Washout of activity. The values given are the percentage of activity that washes out from the heart and liver between 1 and 4 hr after tracer administration as calculated on the whole-body images, as well as the washout from the myocardium between 0.5 and 3.5 hr after tracer administration, as calculated on the SPECT images.

decanoic acid may be caused by the beta-methyl group, which hampers beta-oxidation of the latter compounds.

Second, faster plasma clearance in the glucose-loaded state may derive from lesser leakage of BMIPP or its metabolites from the tissues into the plasma, as will be discussed below.

Effect on Metabolism

The lower levels of PIPA in the plasma that we observed in the glucose-loaded state are testimony to the inhibition of BMIPP metabolism by glucose. Glucose is known to inhibit beta-oxidation (*21*). In the case of BMIPP, such inhibition was demonstrated in a perfused rat heart model (*9*).

Effect on Tissue Radioactivity

We found that tissue activity in the liver and myocardium is higher in the glucose-loaded state. For the heart, this effect could be appreciated on SPECT images, although the differences between the fasted and glucose-loaded states did not reach statistical significance in this small volunteer sample. On projection images, the effect of increased myocardial activity in the glucose-loaded state is attenuated because of decreased activity in the blood.

Increased activity in the heart in the glucose-loaded state is consistent with the weak positive correlation between myocardial BMIPP uptake and plasma insulin levels and also with the weak negative correlation between myocardial BMIPP uptake and serum free fatty acid levels that were observed in 180 patients imaged after fasting (*22*). Increased activity in the heart also concurs with the data obtained in perfused rat hearts (*9*). At the end of 4 hr of perfusion, the fraction of activity remaining in the heart was higher after perfusion with glucose and insulin (55.5 ± 3.0) than after perfusion with oleate (31.6 ± 1.7). Conversely, from the data provided and by using the kinetic model described in the paper on 1-^{11}C-beta-methylheptadecanoic acid, the tissue plateau concentration reached was somewhat lower after glucose/insulin infusion than at baseline in mongrel dogs (*17*).

Higher tissue activity may result either from increased tracer extraction or from delayed washout of activity from the tissues. With respect to the latter, the inhibition of metabolism induced by glucose and insulin may be important. Indeed, in a dog model, metabolites derived from alpha- and beta-oxidation were demonstrated to washout from the myocardium and to constitute an important fraction of the ID, amounting to 6.6% of the intracoronally ID, or ~10% of the dose retained in the myocardium, at 30 min postinjection (*23*). Complete inhibition of the metabolism of BMIPP would, therefore, induce an increase of the activity remaining in the myocardium with the same amount. This compares with the 9% increase of myocardial activity that we found on average in the glucose-loaded state compared with the fasted state.

A second mechanism that may come into play is decreased backdiffusion of BMIPP. Schelbert et al. (*20*) have suggested that glucose and insulin may produce an acceleration of glycolysis and, thereby, make available more glycerol-3-phosphate for esterification of activated fatty acids, causing an extra amount of activity to be trapped into the myocardial cell (*20*). In this respect, it should be noted that despite the decreased extraction of ^{11}C-palmitate that these authors found after glucose and insulin infusion, the size of the late slow phase of the TACs, which reflects the amount of tracer that is sequestered in a slow turnover pool, presumably corresponding to cytosolic triacylglycerols, was higher in the glucose-loaded experiments, not only relative to the amount extracted but also in absolute terms. This may be interpreted as increased intake of fatty acids into the triglyceride pool caused by glucose and insulin.

Intramyocardial Tracer Distribution

Fluorodeoxyglucose (FDG) is more heterogeneously distributed in the fasted state than in the glucose-loaded state (*24*). Because it has been suggested that the heterogeneity of FDG distribution is based on preferential use of fatty acids by the septal myocardium (*25*), we were concerned that the nutritional state would alter the distribution of BMIPP. However, intramyocardial distribution proved not to be different between the fasted and the glucose-loaded state in normal volunteers. This may derive from the fact that BMIPP does not trace fatty acid oxidation as such, but rather its uptake into the myocardium.

Tracer Clearance Between One and Four Hours After Injection

We observed enhanced washout of activity from the myocardium between 1 and 4 hr after injection of ^{123}I-BMIPP after glucose administration. This observation is in keeping with the weak positive correlations between the clearance rate from the myocardium, measured between 15 and 150 min after tracer injection, and plasma insulin and glucose levels and with the negative correlation with serum free fatty acid levels (*22*). Similar enhancement of washout after glucose administration has been demonstrated in ischemic heart disease (*26*). This was explained by accelerated turnover of triglycerides by increased glycerol-3-phosphate levels induced by glucose. An alternative explanation may be derived from our data. Immediately after tracer injection, the influence of glucose on metabolism is still present. BMIPP is taken up by the tissues and may be activated and incorporated into cytosolic triglyceride pools, but the majority is not metabolized through alpha- or beta-oxidation. As time goes by, however, the metabolic effects of the glucose load, including the inhibition of fatty acid metabolism induced by it, decrease. At that point, the excess of BMIPP that has accumulated in the tissues in the triacylglycerol pool may be reintroduced into successive alpha- and beta-oxidation, thereby causing increased washout. Such a release of fatty acid from complex lipids into the fatty acid utilization pathway has been demonstrated with ^{14}C-palmitate (*27*) and the washout kinetics of ^{123}I-BMIPP has been demonstrated mainly to reflect this turnover rate of the triglyceride pool in the cytosol (*28*).

Clinical Implications

Taken together with the data of Fujiwara et al. (*26*) in ischemic heart disease, our results in healthy volunteers indicate that fasting before BMIPP scintigraphy is not mandatory. To the contrary, at the time when SPECT is usually performed (30 min after tracer injection), glucose loading may provide improved ratios between myocardial and blood pool activity, whereas it does not degrade heart-to-liver or heart-to-lung activity ratios.

CONCLUSION

Our results indicate that fasting before BMIPP scintigraphy is not mandatory to obtain adequate SPECT images. At the time when SPECT is usually performed, glucose loading may provide improved ratios between myocardial and blood pool activity.

ACKNOWLEDGMENTS

We thank Dr. Y Yamamichi and colleagues from the Nihon Medi-Physics Central Research Laboratory for providing authentic samples of PIPA.

REFERENCES

1. Knapp FF Jr, Kropp J. Iodine-123-labelled fatty acids for myocardial single-photon emission tomography: current status and future perspectives. *Eur J Nucl Med* 1995;22:361–381.
2. Knapp FF Jr, Franken P, Kropp J. Cardiac SPECT with iodine-123-labeled fatty acids: evaluation of myocardial viability with BMIPP. *J Nucl Med* 1995;36:1022–1030.
3. Tamaki N, Kawamoto M, Yonekura Y, et al. Regional metabolic abnormality in relation to perfusion and wall motion in patients with myocardial infarction: assessment with emission tomography using an iodinated branched fatty acid analog. *J Nucl Med* 1992;33:659–667.
4. De Geeter F, Franken PR, Knapp FF Jr, Bossuyt A. Relationship between blood flow and fatty acid metabolism in subacute myocardial infarction: a study by means of ^{99m}Tc MIBI and ^{123}I beta-methyl iodophenyl pentadecanoic acid. *Eur J Nucl Med* 1994;21:283–291.
5. Franken PR, De Geeter F, Dendale P, Demoor D, Block P, Bossuyt A. Abnormal free fatty acid uptake in subacute myocardial infarction after coronary thrombolysis: correlation with wall motion and inotropic reserve. *J Nucl Med* 1994;35:1758–1765.
6. Franken PR, Dendale P, De Geeter F, Demoor D, Bossuyt A, Block P. Prediction of functional outcome after myocardial infarction using BMIPP and sestamibi scintigraphy. *J Nucl Med* 1996;37:718–722.
7. Knapp FF Jr, Ambrose KR, Goodman MM. New radioiodinated methyl-branched fatty acids for cardiac studies. *Eur J Nucl Med* 1986;12:S39–S44.
8. Knapp FF Jr, Goodman MM, Kirsch G. Iodine-123-labeled DMIPP: a useful new agent to evaluate myocardial fatty acid uptake. *J Nucl Med* 1986;27:521–531.
9. Yamamichi Y, Kusuoka H, Morishita K, et al. Metabolism of iodine-123-BMIPP in perfused rat hearts. *J Nucl Med* 1995;36:1043–1050.
10. Machulla H-J. Carrier-mediated transport of fatty acids causes mismatch between measurements of perfusion and fatty acid metabolism in the myocardium [Letter]. *J Nucl Med* 1996;37:547.
11. De Geeter F. BMIPP and flow tracers in myocardial hypoperfusion [Letter]. *J Nucl Med* 1997;38:1171.
12. Fujibayashi Y, Yonekura Y, Takemura Y, et al. Myocardial accumulation of iodinated beta-methyl-branched fatty acid analog, ^{125}I 15-(p-iodo-phenyl)3-(R,S)-methylpentadecanoic acid (BMIPP), in relation to ATP concentration. *J Nucl Med* 1990;31:1818–1822.
13. Mertens J, Eersels J, Vanryckeghem W. New high yield Cu(I) assisted ^{123}I-radioiodination of 15(p-1-phenyl)-9-methyl pentadecanoic acid, a potential myocardial tracer. *Eur J Nucl Med* 1987;13:159–160.
14. Bax JJ, Veening MA, Visser FC, et al. Optimal metabolic conditions during fluorine-18 fluorodeoxyglucose imaging: a comparative study using different protocols. *Eur J Nucl Med* 1997;24:35–41.
15. De Geeter F, Franken PR, Defrise M, Andries H, Saelens E, Bossuyt A. Optimal collimator choice for sequential iodine-123 and technetium-99m imaging. *Eur J Nucl Med* 1996;23:768–774.
16. Stirner H, Büll U, Kleinhans E. Three-dimensional ROI-based quantification of stress/rest ^{201}Tl myocardial SPECT: presentation of method. *Nuklearmedizin* 1986; 25:128–133.
17. Elmaleh DR, Livni E, Alpert NM, Strauss HW, Buxton R, Fischman AJ. Myocardial extraction of 1-[^{11}C]beta-methylheptadecanoic acid. *J Nucl Med* 1994;35:496–503.
18. Vyska K, Meyer W, Stremmel W, et al. Fatty acid uptake in normal human myocardium. *Circ Res* 1991;69:857–870.
19. Bianco JA, Elmaleh DR, Leppo JA, et al. Effect of glucose and insulin infusion on the myocardial extraction of a radioiodinated methyl-substituted fatty acid. *Eur J Nucl Med* 1986;12:120–124.
20. Schelbert HR, Henze E, Schon HR, et al. Carbon-11 palmitate for the noninvasive evaluation of regional myocardial fatty acid metabolism with positron computed tomography. III. In vivo demonstration of the effects of substrate availability on myocardial metabolism. *Am Heart J* 1983;105:492–504.
21. Stryer L. Fatty acid metabolism. In: Stryer L, *Biochemistry*, 3rd ed. New York: W.H. Freeman and Company; 1988:469–493.
22. Kurata C, Wakabayashi Y, Shouda S, et al. Influence of blood substrate levels on myocardial kinetics of iodine-123-BMIPP. *J Nucl Med* 1997;38:1079–1084.
23. Fujibayashi Y, Nohara R, Hosokawa R, et al. Metabolism and kinetics of iodine-123-BMIPP in canine myocardium. *J Nucl Med* 1996;37:757–761.
24. Gropler RJ, Siegel BA, Lee KJ, et al. Nonuniformity in myocardial accumulation of fluorine-18-fluorodeoxyglucose in normal fasted humans. *J Nucl Med* 1990;31:1749–1756.
25. Schwaiger M, Hicks R. Regional heterogeneity of cardiac substrate metabolism? [Editorial]. *J Nucl Med* 1990;31:1757–1760.
26. Fujiwara S, Takeishi Y, Atsumi H, Takahashi K, Tomoike H. Fatty acid metabolic imaging with iodine-123-BMIPP for the diagnosis of coronary artery disease. *J Nucl Med* 1997;38:175–180.
27. Nellis SH, Liedtke AJ, Renstrom B. Distribution of carbon flux within fatty acid utilization during myocardial ischemia and reperfusion. *Circulation Res* 1991;69:779–790.
28. Morishita S, Kusuoka H, Yamamichi Y, Suzuki N, Kurami M, Nishimura T. Kinetics of radioiodinated species in subcellular fractions from rat hearts following administration of iodine-123-labelled 15-(*p*-iodophenyl)-3-(R,S)-methylpentadecanoic acid (^{123}I-BMIPP). *Eur J Nucl Med* 1996;23:383–389.